Obesity Surgery (2019) 29:2399–2408
https://doi.org/10.1007/s11695-019-03858-9

ORIGINAL CONTRIBUTIONS

Dynamic Adaptive Changes of the Ileum Transposed to the Proximal Small Intestine in Rats

Chang Ho Ahn[1,2] · Sehyun Chae[3,4] · Tae Jung Oh[1,5] · Daehee Hwang[3,6] · Young Min Cho[1,2]

Published online: 29 April 2019

Abstract

Background Ileal transposition (IT) is an experimental surgery to investigate the role of the distal ileum in Roux-en-Y gastric bypass (RYGB) surgery. To systematically investigate the dynamic adaptation process of the ileum after IT, we performed transcriptome analyses of the transposed ileum compared with the ileum in situ at different postoperative time points.

Methods Sprague-Dawley rats fed a chow diet underwent IT or sham surgery. One and 4 weeks after IT or sham surgery, total RNA was extracted from the ileal tissue and subjected to transcriptome analyses using microarray.

Results Principal component analysis showed that the difference between weeks 1 and 4 was the largest, and the differences between the IT and sham groups were larger in week 4 than in week 1. We identified 1792 differentially expressed genes (DEGs) between IT and sham ileal tissues, including 659 and 1133 DEGs in weeks 1 and 4, respectively. Interestingly, only 45 and 24 DEGs were commonly up- or downregulated in weeks 1 and 4, indicating a marked transition during the adaptation process. Functional enrichment and network analyses showed that structural adaptation predominantly occurred in week 1, while metabolic and immune adaptations predominantly occurred in week 4. These analyses further revealed potential components that modulate structural adaptation (e.g., extracellular matrix) in week 1 and metabolic (e.g., glucose transporter) and immune (e.g., Th17 cells) adaptations in week 4.

Conclusions The transposed distal ileum underwent dynamic adaptation processes that may help explain the metabolic changes after RYGB.

Keywords Gut adaptation · Ileal transposition · Transcriptome analysis

Chang Ho Ahn and Sehyun Chae contributed equally to this work.

Electronic supplementary material The online version of this article (https://doi.org/10.1007/s11695-019-03858-9) contains supplementary material, which is available to authorized users.

✉ Daehee Hwang
daehee@snu.ac.kr

✉ Young Min Cho
ymchomd@snu.ac.kr

Chang Ho Ahn
ahncho@gmail.com

Sehyun Chae
implish@postech.ac.kr

Tae Jung Oh
ohtjmd@gmail.com

[1] Department of Internal Medicine, Seoul National University College of Medicine, 101 Daehak-ro, Jongno-gu, Seoul 03080, Republic of Korea

[2] Department of Internal Medicine, Seoul National University Hospital, Seoul, Republic of Korea

[3] Center for Plant Aging Research, Institute for Basic Science, Daegu Gyeongbuk Institute of Science and Technology (DGIST), Daegu, Republic of Korea

[4] Korea Brain Research Institute (KBRI), Daegu, Republic of Korea

[5] Department of Internal Medicine, Seoul National University Bundang Hospital, Seongnam, Republic of Korea

[6] Department of Biological Sciences, Seoul National University, Seoul 08826, Republic of Korea

Introduction

Bariatric surgery has become the most effective treatment option for morbid obesity and its related metabolic conditions [1]. Unveiling the molecular mechanism of bariatric surgery would offer a new therapy for obesity and diabetes. Ileal transposition (IT) is an experimental surgical procedure that is used to investigate the role of the distal small intestine in the metabolic improvements brought about by bariatric surgery [2]. IT translocates a segment of the distal ileum to the upper jejunum distal to the Treitz ligament, which enables a large amount of ingested nutrients to be exposed to the translocated distal ileal tissue, and improves glucose tolerance in both obese and non-obese diabetic rat models [2].

Studies on the mechanisms of bariatric surgery have focused on the traditional organs involving glucose metabolism, which include the pancreas, liver, muscle, and fat [3]. However, the changes in the intestine itself can serve a pivotal role in the metabolic improvements after bariatric surgery [4]. There have been a few studies on the adaptive changes of the transposed ileum. Compared with the ileum in situ (IIS), the transposed ileum (ITR) shows morphological changes, including lengthening of the villi and thickening of the muscle, which is dubbed the jejunization process [5, 6]. Real-time PCR analysis of the ITR showed increased expression of the *Gcg* and *Pyy* genes, accompanied by higher plasma levels of glucagon-like peptide-1 (GLP-1) and peptide YY (PYY) [7], and increased expression of the *Fxr* gene, which implies an alteration in bile acid signaling [8].

The abovementioned results expanded our understanding of the mechanism of IT. However, systematic analysis of the adaptive processes of ITR has rarely been performed. Since the gut adaptation process incorporates many aspects of gut physiology, an unbiased systematic analysis can enable the understanding of such diverse characteristics of the gut adaptation process. Here, as an unbiased systematic analysis, we performed transcriptome analysis of the ITR from IT surgery and of the IIS from sham surgery at two different postoperative time points (weeks 1 and 4) to investigate the gut adaptation process after IT.

Methods

Animals

Male Sprague-Dawley rats aged 13 to 14 weeks were purchased (Orient Bio Inc., Seongnam, Korea). The rats were individually housed and fed a standard chow diet (Purina rat and mouse chow, Purina Korea, Seoul, Korea) ad libitum. After a 1-week acclimation period, rats were randomly selected for sham or IT surgery. For gene expression analysis, rats were sacrificed at 1 and 4 weeks postoperatively. Thus, the study groups consisted of IT and sham groups of postoperative 1-week and 4-week models. The ITR and IIS were harvested from the IT and sham surgery rats, respectively, and fixed in a 10% formalin solution for histologic analysis or frozen in liquid nitrogen and stored at − 70 °C for RNA isolation. To investigate long-term morphological changes in the ITR, the IT-operated rats were killed at 1, 4, 8, 12, and 16 weeks after IT surgery, and the ITR was harvested. Histologic examination and immunohistochemistry of GLP-1 and glucose-dependent insulinotropic polypeptide (GIP) were done for the harvested ileal tissues (Supplementary Method). All animal experiments were approved by the Institutional Animal Care and Use Committee of Seoul National University Hospital (approval no. 13-0273).

Surgical Techniques

The detailed protocol of the surgery was described in our previous study [6]. Briefly, IT or sham surgery was performed after overnight fast under general anesthesia with 2% isoflurane. In the IT surgery, the distal ileal segment located between 5 and 15 cm proximal to the ileocecal valve was resected with intact mesentery and transposed at 10 cm distal to the ligament of Treitz in an isoperistaltic fashion. In the sham surgery, three corresponding transections of the intestine (two for the distal ileum and one for the upper jejunum) were made and repaired in situ. The intestinal anastomosis was made with 6–0 Vicryl. Ceftriaxone (50 mg/kg) was given intramuscularly immediately before laparotomy as a prophylactic antibiotic. Meloxicam (1.5 mg/kg) was given subcutaneously after surgery for postoperative pain control. No oral intake was allowed for 24 h after surgery, and then, liquid meal and water were provided gradually. From postoperative day 3, the standard chow diet and water were given ad libitum. The mortality rates were 18.8% (3/16) and 16% (4/25) for the 1-week and 16-week models, respectively.

Microarray Experiments

The ileal tissue samples stored at − 70 °C were used for the isolation of RNA. Total RNA was isolated from the tissues using an RNeasy Mini kit (Qiagen, Valencia, CA, USA). The integrity of the isolated RNA was analyzed using an Agilent 2100 Bioanalyzer (Agilent Technologies, Palo Alto, CA, USA), and the RNA integrity number (RIN) of all the RNA samples was higher than 9.4, which is larger than the recommended RIN of 8.5 for microarray analysis according to the Agilent protocol for microarray experiments. RNA was reverse transcribed and amplified with the Low Input Quick Amp Labeling Kit (Agilent Technologies, Palo Alto, CA, USA). Complementary RNA was hybridized onto the Agilent rat chip, which includes 62,976 probes corresponding to 19,297 annotated genes. The differentially expressed genes

(DEGs) were defined as false discovery rate ≤ 0.05 and fold change ≥ 1.5. The detailed analytical methods of gene expression data and network analyses are described in Supplementary Method.

Real-time PCR Analysis

The expression levels of representative DEGs associated with the effects of IT surgery were validated using quantitative real-time PCR (qRT-PCR). Complimentary DNA was generated using Superscript II Reverse Transcriptase (Invitrogen, Carlsbad, CA, USA). qRT-PCR was performed with specific primers using SYBR master mix (Takara, Shiga, Japan) and the ABI 7500 Real-Time PCR system (Applied Biosystems, Foster City, CA, USA). The glyceraldehyde-3-phosphate dehydrogenase (GAPDH) expression level was used as the internal control. Nucleotide sequences of the primers are shown in Supplementary Table S1.

Statistical Analysis

With the exception of the microarray data, all other data are shown as the mean ± SEM. When comparing two groups, statistical significance was determined using Student's *t* test. When more than two groups were compared, one-way analysis of variance with Tukey's post hoc test was used. A *P* value < 0.05 was considered statistically significant. Statistical analysis was performed using Prism 7.0 (GraphPad, San Diego, CA, USA).

Results

Metabolic Phenotypes of Postoperative 1-Week and 4-Week Models

We performed IT as illustrated in Fig. 1a. The results of the metabolic studies in the 4-week model were published in our previous paper [6]. Briefly, in the postoperative 4-week model, food intake and body weight decreased, and the levels of plasma glucagon, GLP-1, GLP-2, and PYY increased in the IT group after oral glucose challenge compared with the sham group. However, in the postoperative 1-week model, body weight and food intake were not significantly different between the IT and sham groups (Fig. 1b, c). Plasma glucose, insulin, and gut hormone levels were not significantly different during the mixed meal tolerance test (Fig. 1d–i). These results suggest that the metabolic effects of IT, which were evident at postoperative week 4, were not fully manifested at postoperative week 1.

Morphologic Changes in the Transposed Ileum During the Long-term Postoperative Period

The villi length and muscle thickness increased from 1 to 4 weeks (Fig. 2a–c). However, they showed no further significant changes until 16 weeks. In addition, we examined the density of enteroendocrine K and L cells in the ITR at 1, 4, 8, and 16 weeks after surgery. The density of L cells increased from 1 to 8 weeks and that of K/L cells increased from 1 to 4 weeks (Fig. 2d–f).

Global Gene Expression Profiling of Postoperative 1-Week and 4-Week Models

To systematically examine the molecular nature underlying the aforementioned effects of IT, we performed gene expression profiling of the distal ileum samples from four rats in the IT and sham groups at 1 and 4 weeks after surgery (Fig. 3a). The two time points were determined based on the above observations of the apparent metabolic improvements at week 4 and no further morphologic changes after week 4. Principal component analysis (PCA) showed that the difference was the largest between weeks 1 and 4. In addition, the separation between the IT and sham groups was also apparent at both weeks 1 and 4, although the separation between the IT and sham groups was larger at week 4 than at week 1 (Fig. 3b). Similar patterns were observed in the hierarchical clustering of the gene expression data (Fig. 3c). To identify the genes governing this distinction, we compared gene expression profiles and selected a total of 1792 DEGs between the IT and sham groups in weeks 1 and 4 (Fig. 3d and Supplementary Table S2). Of the genes involved in the enteroendocrine system, *Gip*, *Gcg*, and *Fxr* were found to be upregulated in weeks 1 and 4 (Fig. 3e, f).

Cellular Processes Altered in Postoperative 1-Week and 4-Week Models

To systematically investigate the DEGs, we categorized them into eight clusters (C1–C8) based on their up- and downregulation patterns in weeks 1 and 4 (Fig. 4a). Interestingly, 93.2% of the DEGs showed up- or downregulation uniquely in week 1 or 4. Moreover, among the 121 shared DEGs between weeks 1 and 4, only 45 and 24 (57.0% of 121) were commonly up- and downregulated, respectively. These data suggest that the differential expression of genes by transposition of the distal ileum drastically changes during the course of the early adaptation period. Next, to understand cellular processes associated with the DEGs, we performed enrichment analysis of gene ontology biological processes (GOBPs) for genes in C1–C8 [9] (Supplementary Table S3). Among C1–C8, we focused on GOBPs enriched by four major clusters (C2, C4, C5, and C7) including more than 10% (179 DEGs) of the total number of

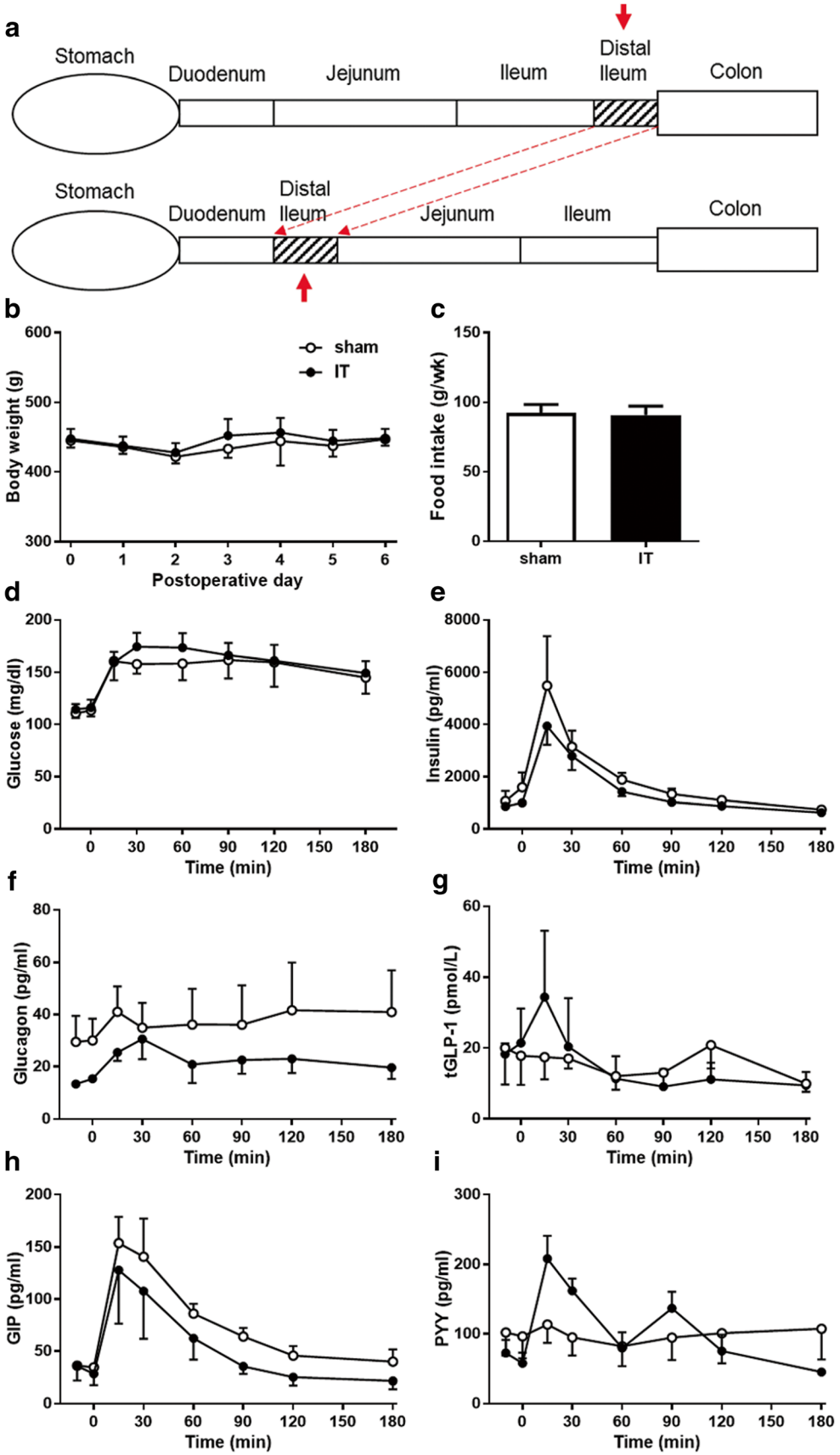
a
Stomach
Duodenum
Jejunum
Ileum
Distal Ileum
Colon
Stomach
Distal Ileum
Duodenum
Jejunum
Ileum
Colon
b
Body weight (g)
sham
IT
Postoperative day
c
Food intake (g/wk)
sham
IT
d
Glucose (mg/dl)
Time (min)
e
Insulin (pg/ml)
Time (min)
f
Glucagon (pg/ml)
Time (min)
g
tGLP-1 (pmol/L)
Time (min)
h
GIP (pg/ml)
Time (min)
i
PYY (pg/ml)
Time (min)

◀ **Fig. 1** Metabolic phenotypes of the postoperative 1-week model. **a** Schematic diagrams for bariatric surgery. The distal ileal segment was first resected. It was then anastomosed in situ in the sham groups and transposed distal to the ligament of Treitz in the IT groups (see arrows). Body weight (**b**) and total food intake after surgery (**c**). Plasma glucose (**d**), insulin (**e**), glucagon (**f**), total GLP-1 (**g**), GIP (**h**), and PYY (**i**) levels during a mixed meal tolerance test with 6 ml/kg of liquid diet (carbohydrate 15 g/dl, protein 3.5 g/dl, and fat 3 g/dl). $N = 6$ and 7 for the sham and IT groups, respectively. Statistical significance was tested using Student's *t* test (**c**) and repeated measures ANOVA with the Sidak post hoc test, but none of the results were statistically significant

DEGs. The upregulated genes in C2 and C4 were mainly associated with cellular processes related to structural adaptation (extracellular matrix organization and cell adhesion), nutrient absorption (response to nutrient and lipid transport), and immune adaptation (wound healing, inflammatory response, neutrophil chemotaxis, macrophage and leukocyte activation, and T cell differentiation) of the ITR (Fig. 4b). Of note, the processes related to structural adaptation and nutrient absorption were upregulated predominantly in week 1, while the processes related to immune adaptation were upregulated predominantly in week 4. On the other hand, the downregulated genes in C5 were mainly associated with fatty acid beta-oxidation and glucose homeostasis, which were related to metabolic adaptations of the ITR (Fig. 4b). These metabolic processes were downregulated predominantly in week 4. These data suggest dynamic regulation of structural, metabolic, and immune adaptations in the early postoperative period after IT.

Network Models of the Adaptation Processes After IT

The GOBP enrichment analysis indicated that IT affected cellular pathways associated with structural, metabolic, and immune adaptations of the ITR. To examine these cellular pathways, we built network models that describe the interactions among the DEGs involved in the aforementioned processes. The network model for structural adaptation (Fig. 5a) showed that extracellular matrix proteins (*Col1a2/4a1/6a1*, *Fn1*, and *Lama2/c1*) and their interacting integrins (*Itga1/a5/a7*) and plasma membrane proteins (*Flna* and *Cav1*) were upregulated at week 1, suggesting their potential roles in the intestinal adaptation after IT [10]. This observation is consistent with the prominent histologic change of the ITR from 1 to 4 weeks.

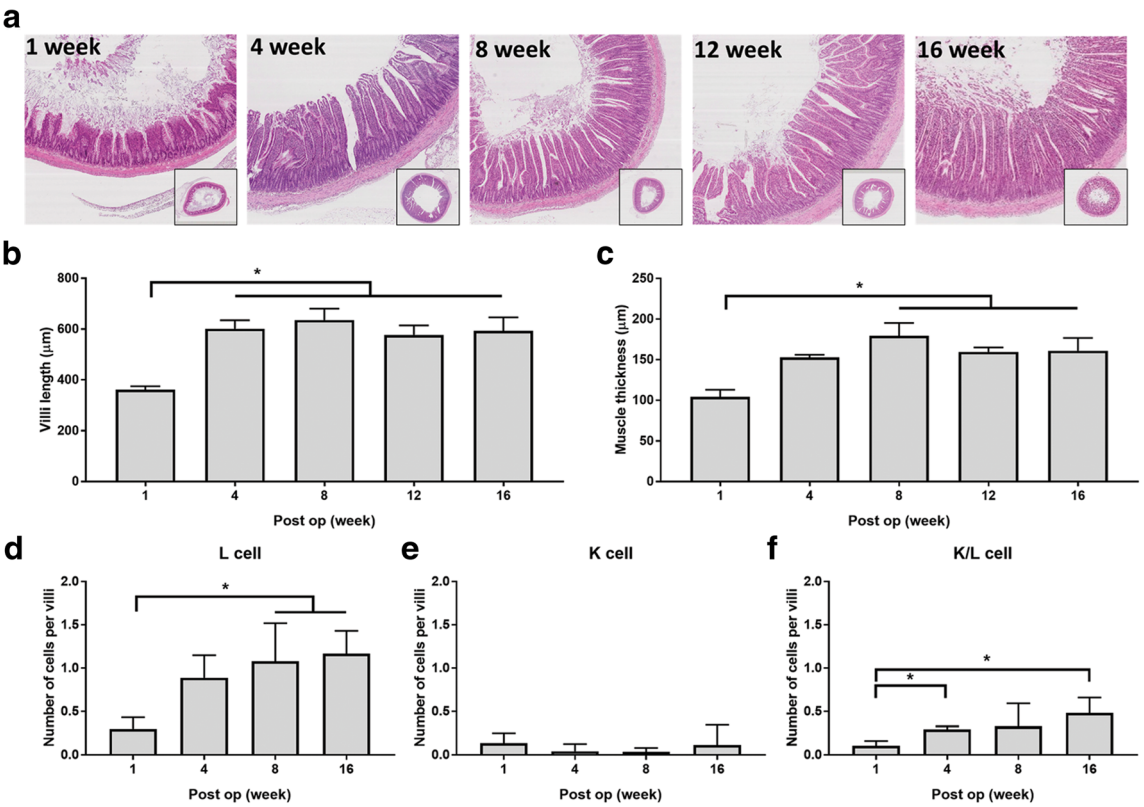

Fig. 2 Morphologic changes in the transposed ileum in the long-term postoperative period. **a** Hematoxylin and eosin–stained section of the transposed ileum at 1 to 16 weeks after IT. Comparison of villi length (**b**) and muscle thickness (**c**) of the transposed ileum ($N = 4$~5) in the IT groups at 1, 4, 8, 12, and 16 weeks after surgery. Comparison of the densities of L (**d**), K (**e**), and K/L (**f**) cells in the transposed ileum in the IT groups at 1, 4, 8, and 16 weeks after surgery ($N = 4$ for 1, 4, 8, and 12 weeks and 5 for 16 weeks). *$P < 0.05$ by one-way ANOVA with Tukey's post hoc test

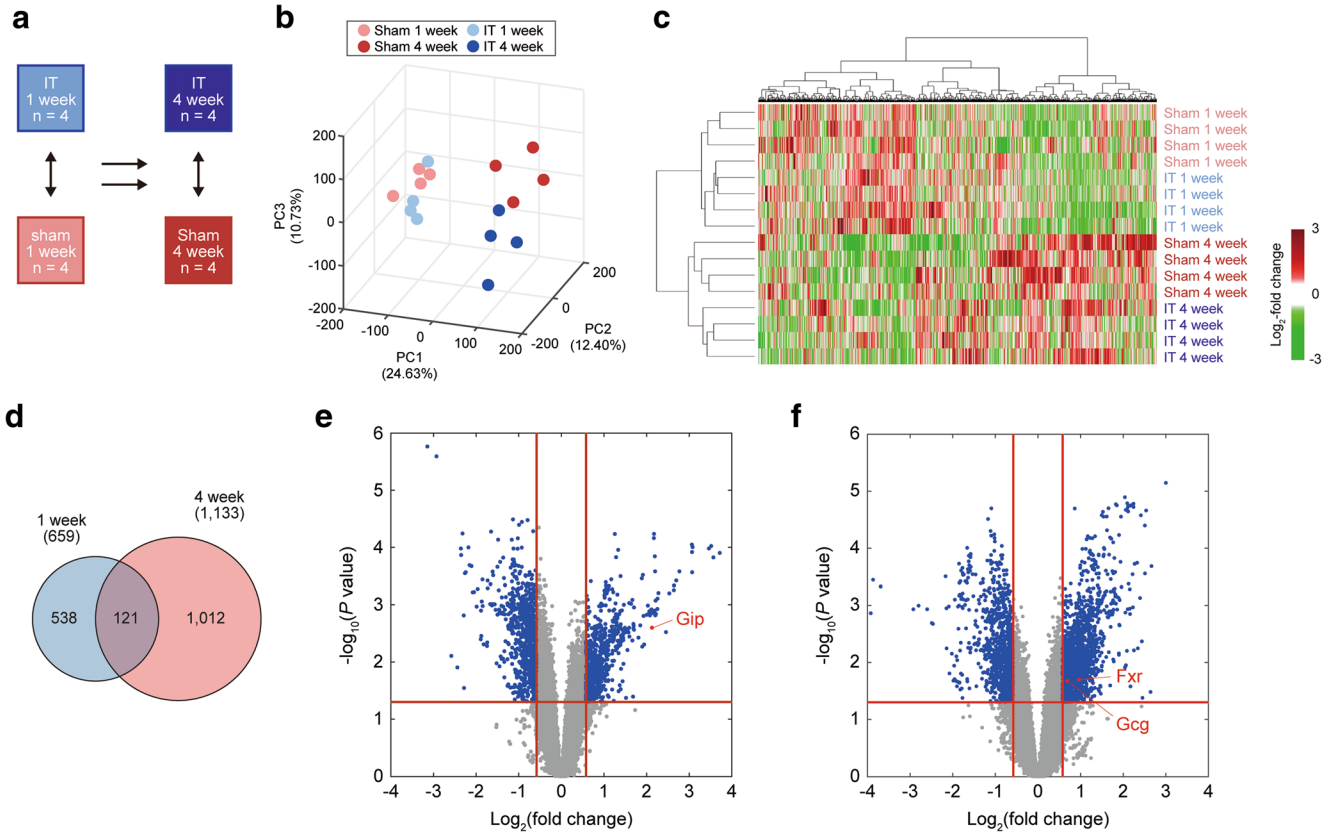

Fig. 3 Differentially expressed genes between the IT and sham groups. **a** Schematic diagrams for tissue microarray analysis. One or 4 weeks after surgery, gene expression profiling of distal ileum tissues obtained from four independent rats in each group was performed. 3-D score plots obtained from principal component analysis (PCA) (**b**) and heat maps showing gene expression patterns obtained from hierarchical clustering (Euclidean distance as a dissimilarity measure and ward linkage method) (**c**). Percentages in parentheses indicate percentages of variance captured by the first three principal components (PC1–PC3). Red and green represent an increase and decrease, respectively, in the expression level of each gene with respect to its median expression level in week 1 or 4. The color bar denotes the gradient of $\log_2$ fold changes of gene expression levels in individual samples with respect to its median expression level. **d** Venn diagram showing relationships between DEGs in weeks 1 and 4. Numbers in parentheses indicate the number of DEGs in weeks 1 and 4. Volcano plots showing DEGs in weeks 1 (**e**) and 4 (**f**). *X*- and *Y*-axes represent the $\log_2$ fold change and the $-\log_{10}(P$ value), respectively. Blue and red dots indicate DEGs and genes previously known to be upregulated after bariatric surgery

The network for immune adaptation (Fig. 5b) showed that many cytokines (*Il1a*, *Il1b*, *Il17a*, and *Il22*) and chemokines (*Ccl3*, *Ccl5*, *Ccl17*, *Ccl19*, *Ccl21*, *Ccl22*, *Cxcl1*, and *Cxcl10*), their receptors (*Il2rb*, *Il6r*, *Il21r*, *Il22ra1*, *Ccr5*, *Ccr9*, *Cxcr3*, *Cxcr4*, and *Cxcr6*), their downstream signaling molecules (*Jak3* and *Stat1*) in the JAK-STAT pathway, and toll-like receptors (*Tlr2* and *Tlr4*) were elevated predominantly in week 4. Then, we examined which types of immune cells were more affected after IT by comparing the differential expression of marker genes for diverse types of immune cells in weeks 1 and 4. The expression of marker genes for T cells, B cells, neutrophils, and macrophages increased in week 4 relative to that of marker genes for other immune cells (Fig. 5c). Interestingly, among the marker genes of T cells, those for Th17 cells, not Th1 and Th2 cells, were significantly upregulated in week 4 (Fig. 5c).

Finally, the network model for metabolic adaptation (Fig. 5d) showed that glucose transporter (*Scl2a2/Glut2*), hexose kinase 3 (*Hk3*), and enolase 3 (*Eno3*) in the glycolytic pathway were elevated from week 1, whereas *G6pc* in the gluconeogenesis pathway was downregulated. On the other hand, fatty acid transporter (*Slc27a2*) and enzymes for fatty acid metabolism (*Cpt1b*, *Acadm*, *Acaa1a*, and *Acaa1b*) were downregulated at week 4. In contrast, amino acid transporters (*Slc7a9* and *Scl1a5*) were upregulated at week 4.

Validation of Differential Expression of Genes Involved in the Adaptation Processes

To validate IT-induced alterations of the aforementioned pathways, we examined differential expression of the following representative genes in the network models by qRT-PCR: *Col1a1* in structural adaptation using the 1-week model; *Ccl5*, *Il1b*, and *Tlr2* in immune adaptation using the 4-week model; and *G6pc*, *Glut2*, *Hk3*, *Slc27a2*, and *Acadm* in metabolic adaptation using the 4-week model. The increased or

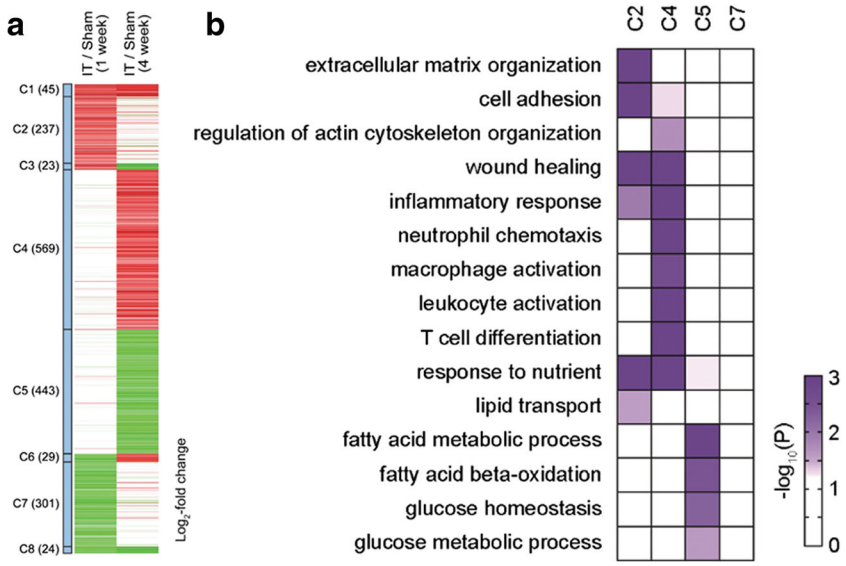

Fig. 4 Clusters of DEGs and their associated cellular processes. **a** Eight clusters (C1–C8) of DEGs defined by up- and downregulation patterns from the comparison of the IT and sham groups (IT/Sham) in weeks 1 and 4. Numbers in parentheses indicate the number of DEGs belonging to the corresponding cluster. Red and green represent increased and decreased expression levels of each gene in the IT groups compared with the sham groups in week 1 or 4. The color bar indicates the gradient of $\log_2$ fold changes between the IT and sham groups. **b** Heat map showing cellular processes (gene ontology biologic processes) enriched by genes in four major clusters (C2, C4, C5, and C7). The color bar denotes the gradient of $-\log_{10}(P)$, where P is the significance of the enrichment obtained by the EASE score method in DAVID

decreased expression of these genes was consistent with the results obtained from microarray experiments (Fig. 6). Log_2 fold changes of these genes in individual samples were significantly correlated with those obtained from microarray experiments (Supplementary Fig. S1).

Discussion

The transposition of the ileum to a proximal part of the small intestine places the ITR in a drastically new environment and assigns an altered physiologic role. To adapt to these new conditions, the ITR undergoes a dynamic transition [5, 6]. However, little is known about cellular processes underlying such dynamic adaptation. Here, histologic analysis of the ITR showed significant changes in tissue morphology up to postoperative week 4. The distribution of GLP-1-positive L cells and both GLP-1- and GIP-positive K/L cells also demonstrated a significant increase during this early postoperative period and no further increase thereafter. Gene expression analyses showed the differential regulation of genes involved in structural, metabolic, and immune adaptations over time. Structural adaptation predominantly occurred at week 1, while metabolic and immune adaptations predominantly occurred at week 4.

According to functional enrichment and network analyses, the most enriched cellular process was extracellular matrix organization, represented by the upregulation of collagen, fibronectin, and laminin (Figs. 3b and 4a) for structural adaptation in postoperative week 1. Consistent with this finding, histologic analysis showed that villi length and muscle thickness increased predominantly from week 1 to 4. In a previous study, after the resection of 80% of the small intestine in rats, the hyperplastic process of the remnant small intestine was nearly complete by 1 week after surgery [11], supporting our finding of structural adaptation at a very early stage after IT.

Few studies have shown direct evidence relating structural adaptation of the intestine with glucose metabolism in animal models of RYGB or vertical sleeve gastrectomy (VSG) [4]. However, several potential mechanisms may explain the roles of structural changes in metabolic improvement after bariatric surgery. The increases in villi length and ileum diameter (Fig. 2a, b) tremendously increase the luminal surface area, which allows efficient absorption of nutrients. A rapid rise in plasma glucose levels after oral ingestion and exaggerated postprandial insulin secretion are consistently observed in patients who have undergone RYGB or VSG [12]. Increased luminal surface area, as well as the upregulation of glucose transporters, *Glut2* in our study, might contribute to these changes. Another potential mechanism is the change in gut permeability. As shown in the network model for structural adaptation (Fig. 4a), the upregulation of laminin (*Lama2* and *Lamc1*) and collagens (*Col4a1* and *Col1a2*), which are the major components of the basement membrane, could enhance the structural integrity of the intestine, thereby reducing gut permeability. We previously reported that plasma endotoxin, which is presumed to be

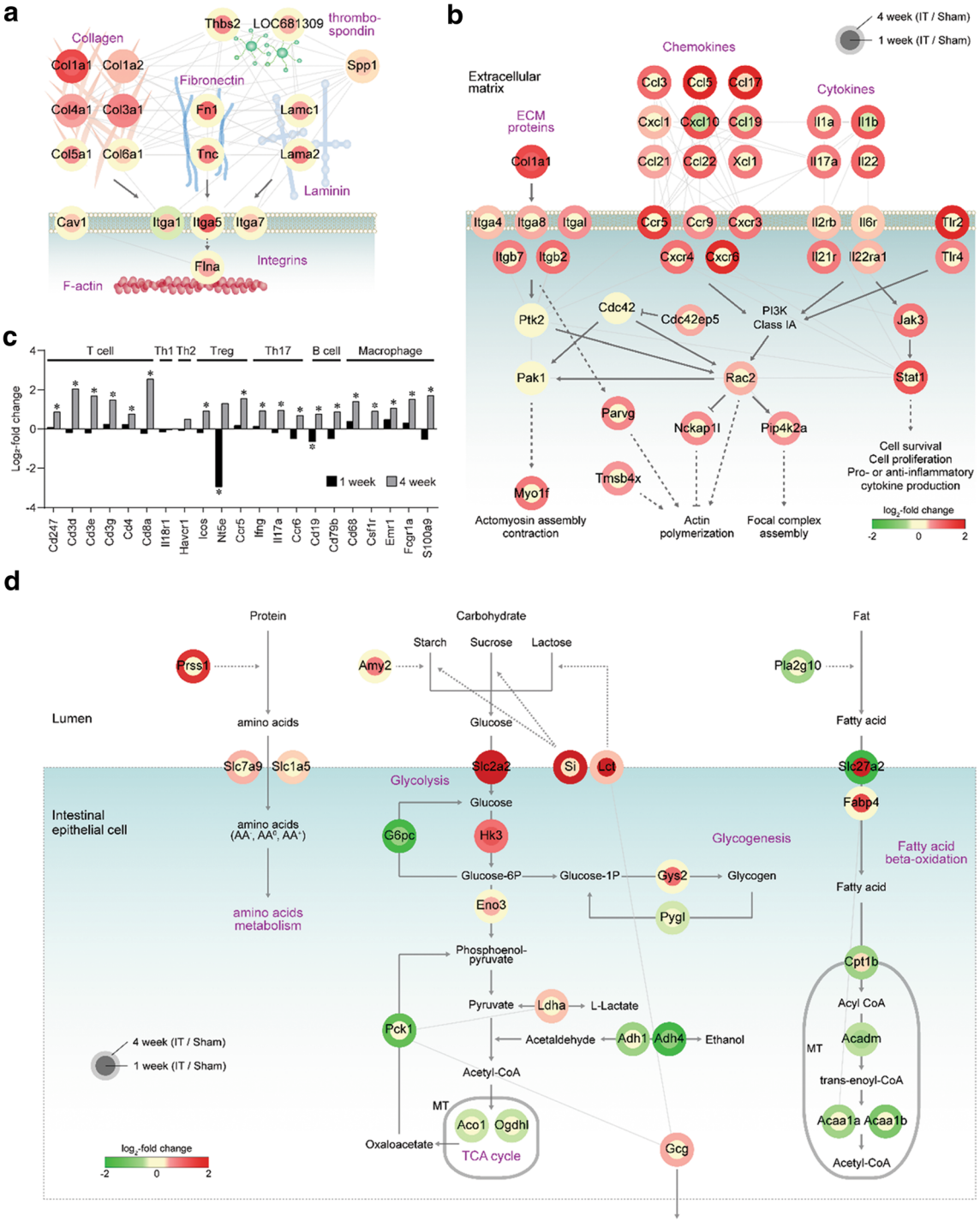

Fig. 5 Network models for the effects of IT. Network models for structural (**a**) and immune adaptation (**b**) of the transposed ileum. Expression of the genetic markers for the different immune cells in weeks 1 and 4 (**c**). Network model for metabolic adaptation of the transposed ileum (**d**). Node center and border colors represent increased (red) and decreased (green) expression levels in the IT groups compared with the sham groups in weeks 1 (center) and 4 (border; see the legend for node center and border). Solid and dotted arrows/inhibition symbols represent direct and indirect activation/inhibition, respectively, obtained from KEGG pathway databases. Gray lines indicate protein-protein interactions obtained from interactome databases ("Methods"). Plasma membranes are denoted by thick gray lines, cytoplasm by a blue background, and extracellular matrix or lumen by a white background

leaked from bacterial endotoxins in the intestinal lumen, was decreased after IT [6]. In human studies, obesity was shown to be associated with increased gut permeability, which can contribute to chronic inflammation through the

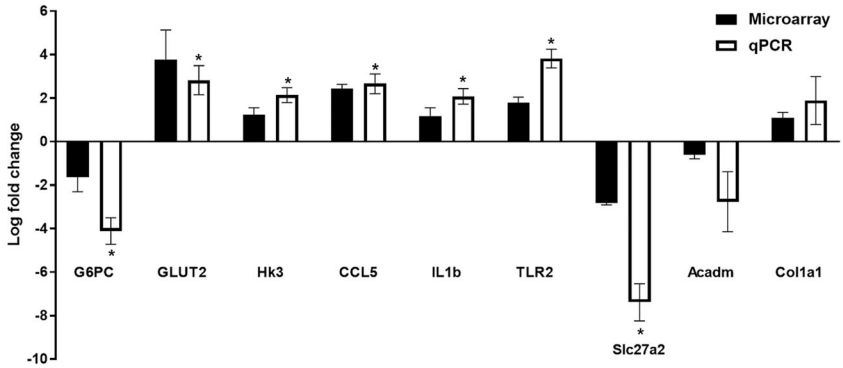

Fig. 6 Validation of the differential expression of representative genes in the key cellular pathways affected by bariatric surgery using qRT-PCR analysis. Data are shown as the mean ± SEM of the $\log_2$ fold change between the IT and sham groups (IT/Sham). $N = 4$ for each group in the microarray experiments and $N = 4$~6 in each group for the qRT-PCR analyses. Gene expression was validated in the 4-week model, except for *Col1a1*. $^*P < 0.05$ comparing the IT and sham groups by Student's *t* test

translocation of gut bacteria or endotoxins [13]. Thus, the structural remodeling of the ITR might contribute to the metabolic benefits by modulating gut permeability.

Our analyses also showed that immune adaptation was apparent at week 4. The upregulation of cytokines, including *Il1b*, *Il17a*, and *Il22*, suggests the possible activation of Th17 cells [14]. Il1b is critical for the differentiation of Th17 in the intestine and Il17a and Il22 are the major effector cytokines of Th17 cells [14]. Th17 cells play an important role in maintaining the mucosal barrier and regulate mucosal immunity against fungi and bacteria in the intestine [14]. Interestingly, a specific gut microbiota promotes Th17 differentiation [15], and the composition of gut microbiota affects the development of Th17 in the intestine [16], which suggests a potential role of Th17 in the host-gut microbiome interaction. In addition, there is a more direct evidence that suggests a role of intestinal Th17 cell in metabolism. The number of Th17 cells was reduced in the small intestine of high fat diet–fed mice [17]. Intriguingly, transfer of gut-tropic Th17 cells to those mice decreased body weight and improved glucose metabolism, which was accompanied by the expansion of commensal gut microbes [17]. In addition, *Tlr2* and *Tlr4* were upregulated in the 4-week model. Toll-like receptors are involved in the interaction between the gut microbiota and host [18]. TLR2 mediates the stimulation of epithelial proliferation by the gut microbiota in the small intestinal mucosa [19]. Gut microbiota is known to play an important role in the pathogenesis of T2DM and mediates key effects of bariatric surgery [20]. The changes in various immunologic signals, including TLRs, might mediate the altered interaction between the gut microbiota and the host, which might be involved in glucose metabolism.

The network model for metabolic adaptation showed upregulation of the glucose transporter *Slc2a2*/*Glut2*, with a 3.7-fold increase in week 1 and a 63.6-fold increase in week 4. GLUT2 can be recruited to the apical membrane of the intestinal epithelium under conditions of high glucose levels in luminal contents [21]. After IT, the ITR is exposed to a luminal content with high concentrations of monosaccharides, which might stimulate the expression of GLUT2 in the epithelium of the ITR. In addition, GLUT2 is involved in glucose sensing and incretin secretion. In an ex vivo study of the rat small intestine, a GLUT2 inhibitor decreased the secretion of GIP, GLP-1, and PYY [22]. In mice lacking GLUT2, postprandial secretion of GLP-1 was impaired [23]. In the ITR, *Hk3*, the gene for the rate-limiting step of glycolysis, was upregulated, and *G6pc*, the gluconeogenesis gene, was downregulated. In this regard, it is noteworthy that increased aerobic glycolysis was reported in the Roux limb of RYGB in rats [24], which might be associated with the improvement of glucose tolerance after RYGB. Similarly, the ITR might undergo increased glucose absorption and glycolysis, which might lead to improved glucose metabolism.

Our study has several limitations. First, the whole thickness of the intestine tissue, instead of a specific layer of the tissue such as the mucosa, was analyzed for microarray. Therefore, our microarray findings reflect overall adaptive changes, which needs to be considered when interpreting the results. Second, we made the same number of cut and anastomosis in the IT and sham surgery groups. Therefore, the intestine of the sham surgery group might exhibit some inflammatory responses. However, our experimental design allows us to examine the changes of gene expression caused by IT regardless of surgical stress. Third, we examined the changes in gene expression only up to 4 weeks. Further adaptive changes in gene expression might occur thereafter, which might affect glucose and energy metabolism after IT. Fourth, we examined the adaptive changes after IT in non-obese non-diabetic rats. Different adaptive changes might be seen if IT was done in obese and/or diabetic rats.

In summary, our transcriptomic analysis showed that diverse and dynamic cellular processes occur in the ITR during the early postoperative adaptive stage. Our findings provide insights into how the ITR adapts to the new environment and

is potentially involved in metabolic improvements, which necessitates further mechanistic investigations.

Funding Information This research was supported by a grant from the Korea Health Technology R&D Project through the Korea Health Industry Development Institute (KHIDI), funded by the Ministry of Health & Welfare, Republic of Korea (HI14C1277); a grant from the Institute for Basic Science (IBS-R013-A1); and a grant from KBRI basic research program through the Korea Brain Research Institute funded by the Ministry of Science and ICT (20180043).

Compliance with Ethical Standards

Competing Interests The authors declare that they have no conflicts of interest.

Statement of Animal Rights/Ethical Approval All animal experiments were approved by the Institutional Animal Care and Use Committee of Seoul National University Hospital (approval no. 13-0273).

References

1. Rubino F, Nathan DM, Eckel RH, Schauer PR, Alberti KG, Zimmet PZ, del Prato S, Ji L, Sadikot SM, Herman WH, Amiel SA, Kaplan LM, Taroncher-Oldenburg G, Cummings DE, Delegates of the 2nd Diabetes Surgery Summit Metabolic surgery in the treatment algorithm for type 2 diabetes: a joint statement by international diabetes organizations. Diabetes Care 2016;39(6):861–877. PubMed PMID: 27222544
2. Oh TJ, Ahn CH, Cho YM. Contribution of the distal small intestine to metabolic improvement after bariatric/metabolic surgery: lessons from ileal transposition surgery. J Diabetes Investig. 2016;7(Suppl 1):94–101.
3. Dirksen C, Jorgensen NB, Bojsen-Moller KN, et al. Mechanisms of improved glycaemic control after Roux-en-Y gastric bypass. Diabetologia. 2012;55(7):1890–901.
4. Seeley RJ, Chambers AP, Sandoval DA. The role of gut adaptation in the potent effects of multiple bariatric surgeries on obesity and diabetes. Cell Metab. 2015;21(3):369–78.
5. Kohli R, Kirby M, Setchell KD, et al. Intestinal adaptation after ileal interposition surgery increases bile acid recycling and protects against obesity-related comorbidities. Am J Physiol Gastrointest Liver Physiol. 2010;299(3):G652–60.
6. Oh TJ, Lee HJ, Cho YM. Ileal transposition decreases plasma lipopolysaccharide levels in association with increased L cell secretion in non-obese non-diabetic rats. Obes Surg. 2016;26(6):1287–95.
7. Strader AD, Vahl TP, Jandacek RJ, et al. Weight loss through ileal transposition is accompanied by increased ileal hormone secretion and synthesis in rats. Am J Physiol Endocrinol Metab. 2005;288(2):E447–53.
8. Mencarelli A, Renga B, D'Amore C, et al. Dissociation of intestinal and hepatic activities of FXR and LXRalpha supports metabolic effects of terminal ileum interposition in rodents. Diabetes. 2013;62(10):3384–93.
9. Huang d W, Sherman BT, Lempicki RA. Systematic and integrative analysis of large gene lists using DAVID bioinformatics resources. Nat Protoc. 2009;4(1):44–57.
10. Schuppan D, Riecken EO. Molecules of the extracellular matrix: potential role of collagens and glycoproteins in intestinal adaptation. Digestion. 1990;46(Suppl 2):2–11.
11. O'Connor TP, Lam MM, Diamond J. Magnitude of functional adaptation after intestinal resection. Am J Phys. 1999;276(5 Pt 2):R1265–75.
12. Madsbad S, Dirksen C, Holst JJ. Mechanisms of changes in glucose metabolism and bodyweight after bariatric surgery. Lancet Diabetes Endocrinol. 2014;2(2):152–64.
13. Cox AJ, West NP, Cripps AW. Obesity, inflammation, and the gut microbiota. Lancet Diabetes Endocrinol. 2015;3(3):207–15.
14. Blaschitz C, Raffatellu M. Th17 cytokines and the gut mucosal barrier. J Clin Immunol. 2010;30(2):196–203.
15. Ivanov II, Frutos Rde L, Manel N, et al. Specific microbiota direct the differentiation of IL-17-producing T-helper cells in the mucosa of the small intestine. Cell Host Microbe. 2008;4(4):337–49.
16. Gaboriau-Routhiau V, Rakotobe S, Lecuyer E, et al. The key role of segmented filamentous bacteria in the coordinated maturation of gut helper T cell responses. Immunity. 2009;31(4):677–89.
17. Hong CP, Park A, Yang BG, et al. Gut-specific delivery of T-helper 17 cells reduces obesity and insulin resistance in mice. Gastroenterology. 2017;152(8):1998–2010.
18. Yiu JH, Dorweiler B, Woo CW. Interaction between gut microbiota and toll-like receptor: from immunity to metabolism. J Mol Med (Berl). 2017;95(1):13–20.
19. Hormann N, Brandao I, Jackel S, et al. Gut microbial colonization orchestrates TLR2 expression, signaling and epithelial proliferation in the small intestinal mucosa. PLoS One. 2014;9(11):e113080.
20. Tremaroli V, Karlsson F, Werling M, et al. Roux-en-Y gastric bypass and vertical banded gastroplasty induce long-term changes on the human gut microbiome contributing to fat mass regulation. Cell Metab. 2015;22(2):228–38.
21. Kellett GL, Helliwell PA. The diffusive component of intestinal glucose absorption is mediated by the glucose-induced recruitment of GLUT2 to the brush-border membrane. Biochem J. 2000;350(Pt 1):155–62.
22. Cani PD, Holst JJ, Drucker DJ, et al. GLUT2 and the incretin receptors are involved in glucose-induced incretin secretion. Mol Cell Endocrinol. 2007;276(1–2):18–23.
23. Mace OJ, Schindler M, Patel S. The regulation of K- and L-cell activity by GLUT2 and the calcium-sensing receptor CasR in rat small intestine. J Physiol. 2012;590(12):2917–36.
24. Saeidi N, Meoli L, Nestoridi E, et al. Reprogramming of intestinal glucose metabolism and glycemic control in rats after gastric bypass. Science. 2013;341(6144):406–10.